Supporting Information

A *meta*-alkylthio-phenyl Chain Substituted Small Molecule Donor as the Third Component for High-Efficiency Organic Solar Cells

Chenyang Zhang,[a] Jing Li,[a] Lei Ji,[a] Hanlin Hu,*[b] Gang Li,*[c] Kai Wang *[a]

[a] *Institute of Flexible Electronics (IFE), Northwestern Polytechnical University (NPU), Xi'an 710072, China. Email: kaiwang@nwpu.edu.cn*

[b] *Hoffman Institute of Advanced Materials, Shenzhen Polytechnic, 7098 Liuxian Boulevard, Shenzhen 518055, China. Email: hanlinhu@szpt.edu.cn*

[c] *Department of Electronic and Information Engineering, Research Institute for Smart Energy (RISE), The Hong Kong Polytechnic University, Hung Hom, Kowloon, Hong Kong, China. Email: gang.w.li@polyu.edu.hk (G. Li)*

1. General Experimental Details

Methods and Materials: All reagents from commercial sources were used without further purification. Solvents were dried and purified using standard techniques. Reactions were carried out under nitrogen atmosphere when appropriate. All compounds were characterized by NMR spectroscopy on Bruker Avance III Ultrashield Plus instruments using a 500 MHz proton frequency at the given temperatures. The spectra were referenced to the internal standard TMS. The photophysical and electrochemical properties of the materials were measured on UV-visible-near infrared spectrograph (Agilent Cary 60 spectrometer) and electrochemistry workstation (CHI660A, Chenhua Shanghai), respectively. The DSC samples were prepared by scraping and collecting the annealed blend films from glass, which were prepared by coating and drying the blend solutions. Atomic force microscopy (AFM) images were characterized with a Veeco Multi-Mode 8 in a tapping mode. GIWAXS measurements were carried out with a Xeuss 2.0 WAXS/SAXS laboratory beamline using a Cu X-ray source (8.05 keV, 1.54 Å) and a Pilatus3R 300K detector. GIWAXS samples were prepared on silicon substrate by spin coating.

2. Reported second SM donor

Table S1. Photovoltaic parameters of the reported PM6:Y6-based TOSCs based on a SM molecule as second donor.

SM donor	V_{OC} [V]	J_{SC} [mA cm^{-2}]	FF [%]	PCE [%]	Ref.
SM1	0.831	25.7	77.5	16.55	[1]
BPR-SCl	0.87	25.77	75.0	16.74	[2]
ECTBD	0.848	25.54	76.24	16.51	[3]
BTR	0.839	25.8	76.7	16.6	[4]
DRTB-T-C4	0.85	24.79	81.3	17.13	[5]
$TiC1_2$	0.853	26.80	75.4	17.25	[6]
BTTzR	0.87	26.2	77.7	17.70	[7]
BTBR-2F	0.859	27.30	74.11	17.38	[8]
BR1	0.859	26.49	75.7	17.23	[9]
DFBT-TT6	0.845	26.56	76	17.05	[10]
DR8	0.859	25.89	75.22	16.73	[11]
TTBT-R	0.863	27.38	76.46	18.07	[12]
BTID-2F	0.848	27.66	76.36	17.98	[13]

3. Synthetic Procedures

Compound 1 and 2 were synthesized according to previously reported methods.[14,15]

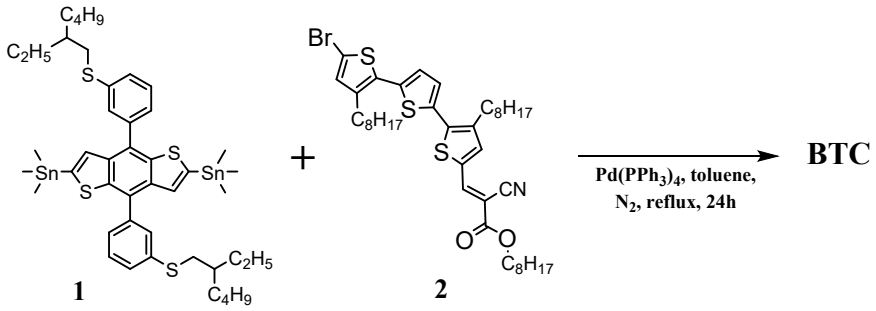

Scheme S1. The synthetic route of BTC.

(5*Z*,5'*Z*)-5,5'-(((4,8-bis(3-((2-ethylhexyl)thio)phenyl)benzo[1,2-*b*:4,5-*b*']dithiophene-2,6-diyl)-bis(3,3''-dioctyl-[2,2':5',2''-terthiophene]-5'',5-diyl))(2*E*,2'*E*)-bis(octyl-2-cyanoacrylate) (BTC)**:** A mixture of (1) (0.086 g, 0.09 mmol), (2) (0.171 g, 0.225 mmol) and $Pd(PPh_3)_4$ (1.56 mg, 0.00135 mmol) in a flask was subjected to three vacuum/nitrogen cycles, and degassed toluene (3.0 mL) was added to the flask. The reaction mixture was stirred in an oil bath for 24 hours at 120 °C. The solvent was removed and the residue was purified via column chromatography over SiO_2 using CH_2Cl_2/hexanes (6/4) as the eluent. The product fractions were pooled, concentrated, purified by recycling SEC ($CHCl_3$), yielding BTC as a dark purple solid (108 mg, 60%). ^{1}H NMR (500 MHz, $CDCl_3$): δ 8.22 (s, 2H), 7.68 (s, 2H), 7.62 (s, 2H), 7.55 – 7.49 (m, 6H), 7.34 (s, 2H), 7.31 (d, J = 4.0 Hz, 2H), 7.14 (d, J = 4.0 Hz, 2H), 7.11 (s, 2H), 4.31 (t, J = 6.5 Hz, 4H), 3.03 (d, J = 6.5 Hz, 4H), 2.85 (t, J = 7.5 Hz, 4H), 2.78 (t, J = 7.5 Hz, 4H), 1.79 – 1.66 (m, 14H), 1.53 – 1.26 (m, 78H), 0.96 – 0.86 (m, 28H). ^{13}C NMR (100 MHz, $CDCl_3$): δ 163.21, 146.01, 141.65, 141.32, 140.84, 140.82, 140.65, 139.51, 139.19, 138.37, 137.97, 137.67, 137.04, 135.73, 134.42, 133.07, 130.37, 129.60, 129.54, 128.70, 128.51, 128.35, 126.40, 126.33, 118.60, 116.08, 97.84, 66.66, 39.03, 37.89, 37.87, 32.51, 31.96, 31.93, 31.86, 30.52, 30.32, 30.30, 29.76, 29.71, 29.60, 29.53, 29.48, 29.44, 29.35, 29.33, 29.31, 29.27, 29.24, 28.87, 28.64, 25.89, 25.76, 23.08, 22.75, 22.74, 14.20, 14.16, 10.92. HRMS (+APCI, m/z): calcd. for $C_{118}H_{156}N_2O_4S_{10}$ $[M+H]^+$: 1987.16; found 1987.03.

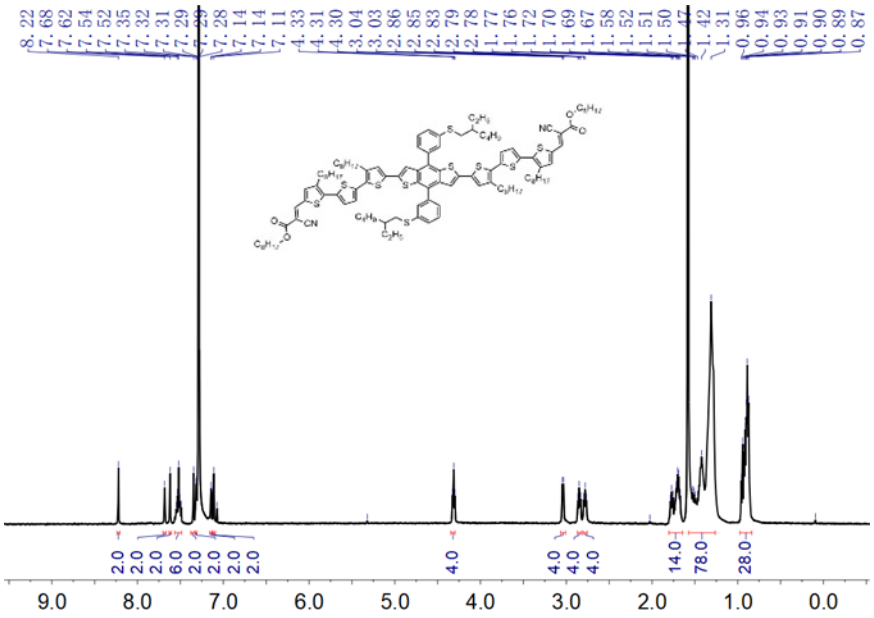

Fig. S1. ^{1}H NMR spectrum of BTC in $CDCl_3$.

Fig. S2. ^{13}C NMR spectrum of BTC in $CDCl_3$.

4. High-resolution mass spectrometry (HRMS)

The High-resolution mass spectrometry (HRMS) data was recorded using Agilent 6550 iFunnel Q-TOF.

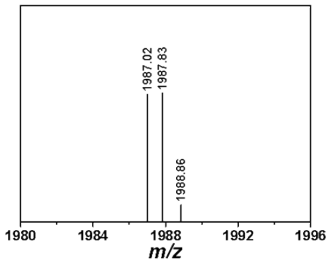

Fig. S3. High-resolution mass spectrometry (HRMS) of BTC.

5. Thermogravimetric analyses (TGA)

Thermogravimetric analyses (TGA) was performed with a TA TGA 50 under nitrogen atmosphere, with a set ramp rate of 10 °C/min, and using Al_2O_3 (alox) crucibles.

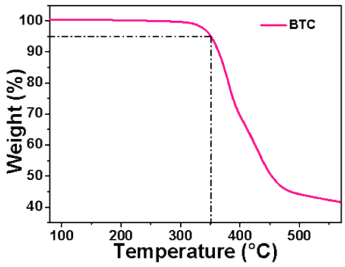

Fig. S4. Thermogravimetric analyses (TGA) of BTC.

6. Computational analyses and Cyclic voltammetry (CV)

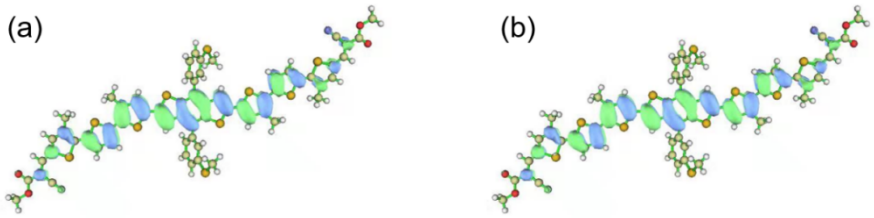

E_{HOMO}= -5.33eV E_{LUMO}= -3.12eV

Fig. S5. The distribution of frontier molecular orbitals (HOMO and LUMO) of BTC.

The electrochemical properties of the materials was measured by electrochemistry workstation (CHI660A, Chenhua Shanghai).

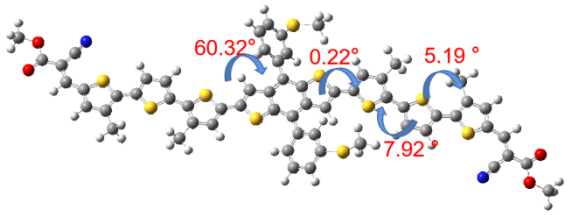

Fig. S6. The molecular conformation and dihedral angles of BTC.

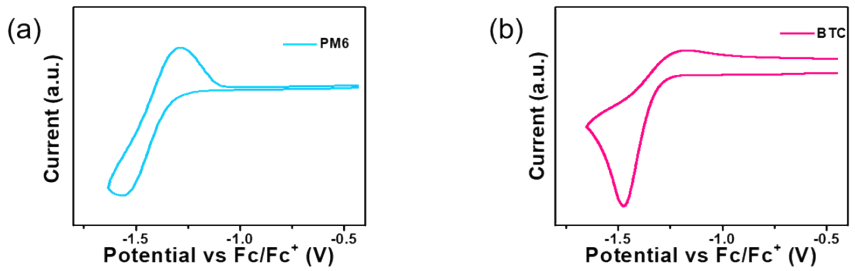

Fig. S7. The results of cyclic voltammetry (CV) of (a) PM6, (b) BTC.

7. Device Fabrication

The solar cells were prepared on glass substrates with tin-doped indium oxide (ITO, 15 Ω sq^{-1}) patterned on the surface (device area: 0.04 cm^2). Substrates were first scrubbed with dilute Extran 300 detergent solution to remove organic residues before immersing in an ultrasonic bath of dilute Extran 300 for 15 min. Samples were rinsed in flowing deionized water for 5 min before being sonicated (Branson 5510) for 15 min each in successive baths of acetone and isopropanol. Next, the samples were exposed to a UV−ozone plasma for 30 min. A ZnO precursor solution was spin coated onto a cleaned ITO, subsequently annealed at 130℃ for 30 min in the air to obtain a ZnO-covered ITO., and then transferred into a dry nitrogen glovebox (< 0.01 ppm O_2).

The chloroform solution (16 mg mL^{-1} in total) with 0.5 vol% of 1-CN was spin-coated on ZnO layer with 4000 rpm for 30 s to obtain a photosensitive active layer. The active layers were spin-cast from the solutions at an optimized speed of 4000 rpm for BTC in a time period of 30 s, using a programmable spin coater from Specialty Coating Systems (Model G3P-8), resulting in films of ca. 100 nm in thickness. At last, the MoO_3 layer and Ag electrode were slowly evaporated onto the surface of active layer under a vacuum pressure of 3×10^{-4} Pa.

J-V measurements of solar cells were performed in the air with a Keithley 2400 source meter and an Oriel Sol3A Class AAA solar simulator calibrated to 1 sun, AM1.5 G, with a KG-5 silicon reference cell certified by Newport. The external quantum efficiency (EQE) measurements were performed at zero bias by illuminating the device with monochromatic light supplied from a Xenon arc lamp in combination with a dual-grating monochromator. The number of photons incident on the sample was calculated for each wavelength by using a silicon photodiode calibrated by NIST.

Table S2. Device parameters of PM6:BTC:Y6 (0.5%CN) with different $D_1/D_2/A$ weight ratio under thermal annealing at 80℃ for 15 min.

D_1:D_2:A	V_{OC} [V]	J_{SC} [mA cm^{-2}]	FF [%]	PCE [%]
1:0.1:1.2	0.828	27.93	72.06	16.67
1:0.15:1.2	0.837	27.56	72.82	16.81
1:0.2:1.2	0.839	27.31	72.41	16.58

Table S3. Device parameters of PM6:BTC:Y6 (0.5%CN) with different thermal annealing temperature.[a]

Temperature [℃]	V_{OC} [V]	J_{SC} [mA cm^{-2}]	FF [%]	PCE [%]
70	0.841	28.04	72.09	17.01
80	0.839	27.96	73.08	17.14
90	0.834	28.24	73.51	17.32
100	0.824	28.13	74.16	17.20

[a] The ternary ratio is 1:0.15:1.2 for PM6:BTC:Y6 (0.5%CN).

Table S4. Device parameters of BTC:Y6 with different additive under thermal annealing at 100℃ for 15 min.

Additive	V_{OC} [V]	J_{SC} [mA cm^{-2}]	FF [%]	PCE [%]
No additive	0.673	20.71	47.02	6.55
0.1%CN	0.632	19.42	42.48	5.21
0.2%CN	0.629	18.21	44.36	5.08
0.3%CN	0.555	15.95	38.42	3.40

[a] The binary ratio is 2:1 for BTC:Y6.

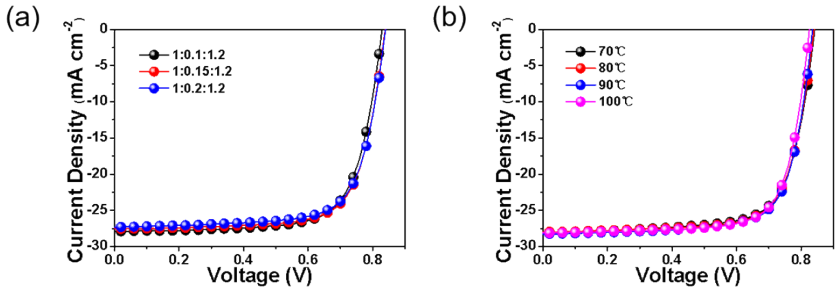

Fig. S8. Current density-voltage (J–V) curves of PM6:BTC:Y6 with different (a) $D_1/D_2/A$ weight ratio and (b) thermal annealing temperature.

Table S5. Device parameters of BTC:Y6 with different D/A weight ratio under thermal annealing at 100℃ for 15 min.

D:A	V_{OC} [V]	J_{SC} [mA cm^{-2}]	FF [%]	PCE [%]
1:1	0.678	18.13	39.98	4.91
1.5:1	0.687	20.22	45.56	6.33
2:1	0.698	20.11	48.19	6.76
2.5:1	0.690	20.53	45.61	6.46

Table S6. Device parameters of BTC:Y6 with different thermal annealing temperature.[a]

Temperature [°C]	V_{OC} [V]	J_{SC} [mA cm^{-2}]	FF [%]	PCE [%]
70	0.810	15.17	32.95	4.05
80	0.801	18.28	51.06	7.48
90	0.733	19.95	48.94	7.16
100	0.703	19.35	48.61	6.61

[a] The binary ratio is 2:1 for BTC:Y6.

8. Absorption Coefficients

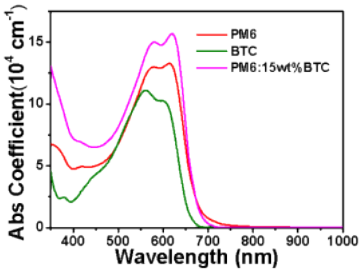

Fig. S9. Absorption coefficient of neat PM6, BTC and PM6:BTC blend films.

9. Differential Scanning Calorimetry (DSC)

The differential scanning calorimetric (DSC) measurements was carried out on a DSC Q10 differential scanning calorimeter instrument under nitrogen gas flow with a 20 °C/min heating rate. The DSC samples were prepared by scraping and collecting the annealed blend films from glass, which were prepared by coating and drying the blend solutions.

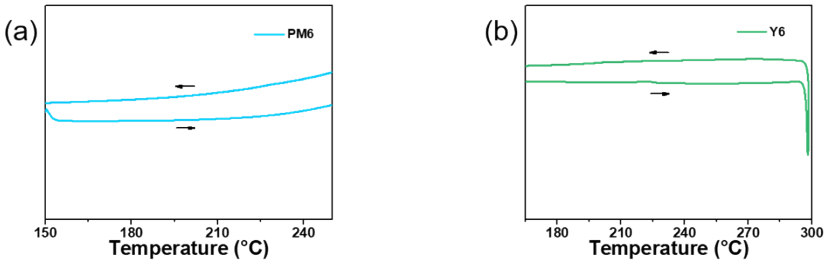

Fig. S10. Differential scanning calorimetry (DSC) traces of (a) PM6, (b) Y6.

10. Atomic Force Microscopy (AFM) Imaging

A Dimension Icon atomic force microscope (AFM) from Bruker was used to image the active layers in tapping mode.

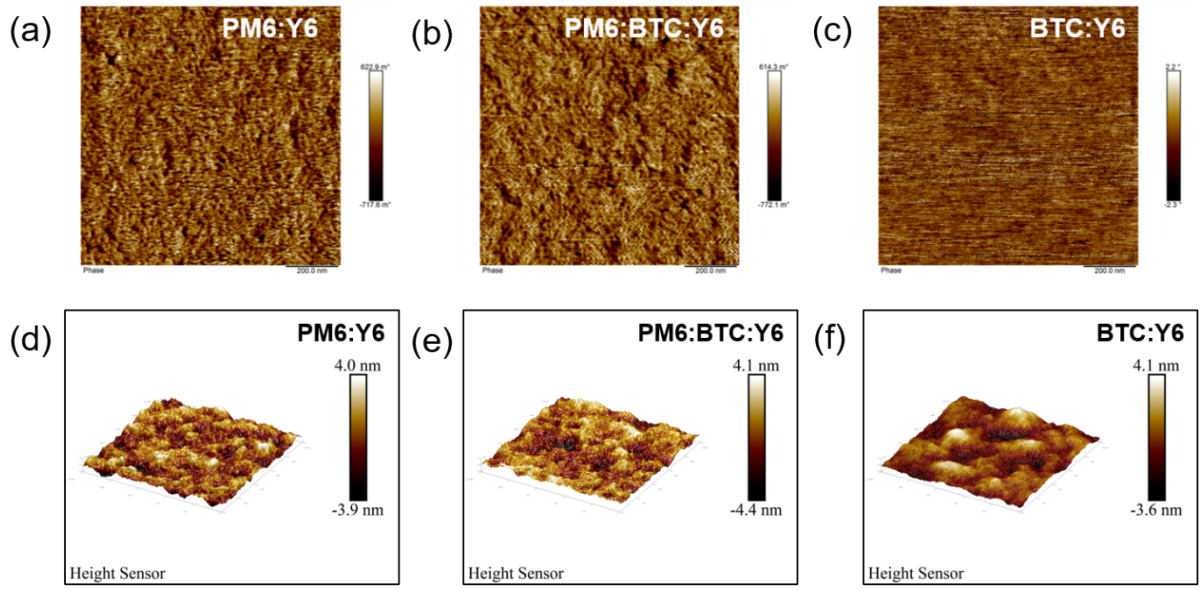

Fig. S11. AFM 3D images (1x1 μm^2) for optimized BHJ thin films. AFM phase and 3D images of (a and d) binary, (b and e) optimal ternary blends (1:0.15:1.2), and (c and f) BTC:Y6 (2:1).

11. Grazing Incidence Wide-angle X-ray Scattering (GIWAXS)

GIWAXS measurements were carried out with a Xeuss 2.0 WAXS/SAXS laboratory beamline using a Cu X-ray source (8.05 keV, 1.54 Å) and a Pilatus3R 300K detector.

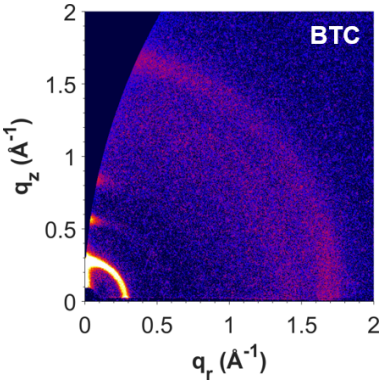

Fig. S12. 2D GIWAXS images of BTC pure film.

Table S7. The detailed parameters of corresponding 2D GIWAXS in the OOP direction**.**

Sample	Q [Å−1]	D [Å]	FWHM [Å−1]	CCL [Å]
PM6:Y6	1.75	3.58	0.262	23.96
PM6:BTC:Y6	1.70	3.69	0.257	24.43

Table S8. The detailed parameters of corresponding 2D GIWAXS in the IP direction**.**

Sample	Q [Å^{-1}]	D [Å]	FWHM [Å^{-1}]	CCL [Å]
PM6:Y6	0.29	21.65	0.154	40.77
PM6:BTC:Y6	0.29	21.65	0.105	59.80

12. SCLC Mobility

The hole and electron mobilities of BTC in optimized BHJ thin films were determined by fitting the dark current to the space-charge-limited current (SCLC) model using the following diode configuration: Glass/ITO/PEDOT:PSS/BHJ/MoO_3/Ag for hole-only diode, and Glass/ITO/ZnO/BHJ/PFN-Br/Ag for electron-only diode. The ITO substrates, bottom PEDOT:PSS layers and BHJ layers were prepared. A top MoO_3 layer (7.5 nm) was used as the electron-blocking layer and Silver cathode (100nm) were thermally evaporated through a shadow mask defining an active area of 0.04 cm^2 in the hole-only diodes. For electron-only device, the ZnO layer was spin coated by solution-processed method on top of ITO substrate. A PFN-Br layer (ca. 5nm) as the hole-blocking layer and Ag layer (100nm) as the anode were then thermally evaporated. The electric-field-dependent SCLC mobility was estimated from Equation 1.

$$J(V) = \frac{9}{8}\varepsilon_0\varepsilon_r\mu_0 exp\left(0.89\beta\sqrt{\frac{V - V_{bi}}{L}}\right)\frac{(V - V_{bi})^2}{L^3} \quad (1)$$

Definition	Variable	Units
zero-field mobility	μ_0	$cm^2\ V^{-1}\ s^{-1}$
film thickness	L	cm
dark current density	J	$mA\ cm^{-2}$
voltage	V	V
vacuum permittivity	ε_0 (88.54×10^{-12})	$mA\ s\ V^{-1}\ cm^{-1}$
dielectric constant	ε_r (3)	
field activation factor	β	$cm^{1/2}\ V^{-1/2}$

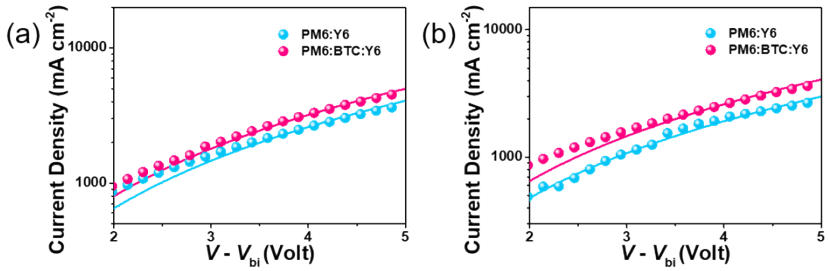

Fig. S13. Dark current density-voltage characteristics at room temperature of optimized binary and ternary films for (a) hole-only diodes and (b) electron-only diodes. Note: The experimental data is fitted using the single-carrier SCLC model (solid lines). The solid lines are fits to the experimental data according to Equation.

13. Photoluminescence Spectra Data

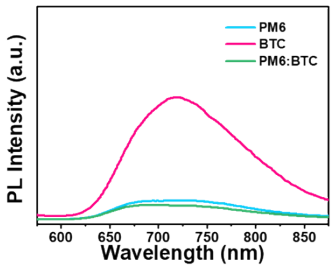

Fig. S14 Photoluminescence spectra of PM6, BTC and PM6:BTC (1:0.15) films.

14. Additional PV Device Performance Data

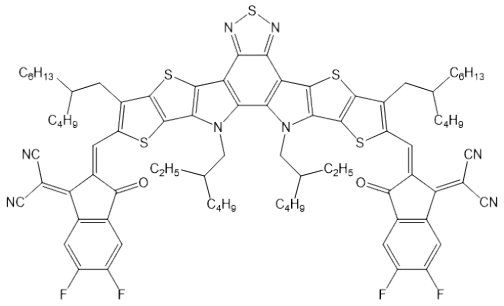

Fig. S15. Chemical structures of L8-BO.

Table S9. Device parameters of PM6:BTC:L8-BO (0.3%DIO) with different D_1/D_2/A weight ratio under thermal annealing at 100°C for 10 min.

D_1:D_2:A	V_{OC} [V]	J_{SC} [mA cm^{-2}]	FF [%]	PCE [%]
1:0.1:1.2	0.892	26.65	75.35	17.92
1:0.15:1.2	0.894	26.67	76.08	18.13
1:0.2:1.2	0.896	26.60	73.87	17.60

Table S10. Device parameters of PM6:BTC:L8-BO (0.3%DIO) with different thermal annealing temperature.[a]

Temperature [°C]	V_{OC} [V]	J_{SC} [mA cm^{-2}]	FF [%]	PCE [%]
70	0.899	26.52	74.05	17.65
80	0.898	26.67	75.46	18.07
90	0.896	26.84	76.50	18.41
100	0.894	26.67	76.13	18.15

[a] The ternary ratio is 1:0.15:1.2 for PM6:BTC:L8-BO (0.3%DIO).

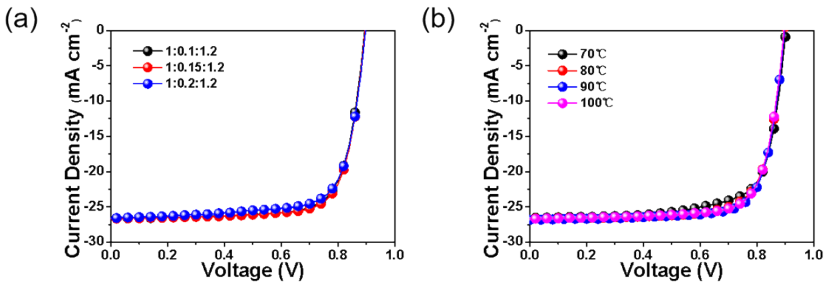

Fig. S16. Current density-voltage (*J*–*V*) curves of PM6:BTC:L8-BO with different (a) $D_1/D_2/A$ weight ratio and (b) thermal annealing temperature.

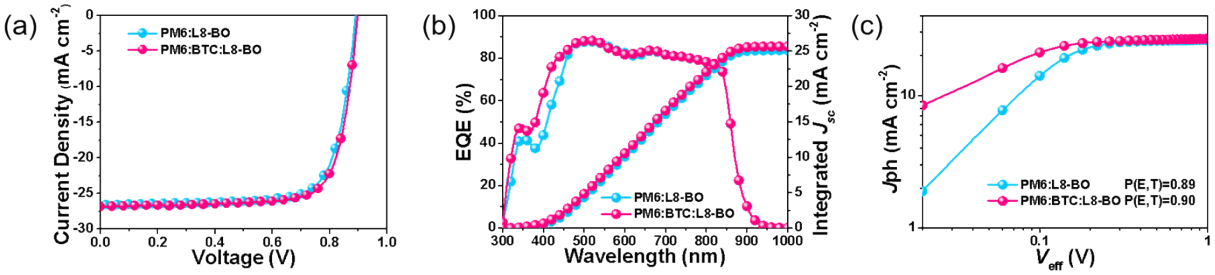

Fig. S17. (a) Current density-voltage (*J*–*V*) curves, (b) EQE spectra of the binary and the optimized ternary devices under AM 1.5G illumination (100 mW cm^{-2}) and (c) The J_{ph}-V_{eff} curves of PM6:L8-BO binary and BTC-based ternary OSCs.

15. References

1 T. Yan, J. Ge, T. Lei, W. Zhang, W. Song, B. Fanady, D. Zhang, S. Chen, R. Peng and Z. Ge, *J. Mater. Chem. A*, 2019, **7**, 25894–25899.

2 X. Chen, Q. Zhang, D. Wang, X. Xu, Z. Wang, Y. Li, H. Zhu, X. Lu, W. Chen, H. Qiu and C.-Z. Li, *Sol. RRL*, 2020, **4**, 2000537.

3 S. Chen, T. Yan, B. Fanady, W. Song, J. Ge, Q. Wei, R. Peng, G. Chen, Y. Zou and Z. Ge, *Sci. China Chem.*, 2020, **63**, 917–923.

4 C. Yan, H. Tang, R. Ma, M. Zhang, T. Liu, J. Lv, J. Huang, Y. Yang, T. Xu, Z. Kan, H. Yan, F. Liu, S. Lu and G. Li, *Adv. Sci.*, 2020, **7**, 2000149.

5 D. Li, L. Zhu, X. Liu, W. Xiao, J. Yang, R. Ma, L. Ding, F. Liu, C. Duan, M. Fahlman and Q. Bao, *Adv. Mater.*, 2020, **32**, 2002344.

6 W. Tang, W. Peng, M. Zhu, H. Jiang, W. Wang, H. Xia, R. Yang, O. Inganäs, H. Tan, Q. Bian, E. Wang and W. Zhu, *J. Mater. Chem. A*, 2021, **9**, 20493–20501.

7 Q. Liu, Y. Wang, J. Fang, H. Liu, L. Zhu, X. Guo, M. Gao, Z. Tang, L. Ye, F. Liu, M. Zhang and Y. Li, *Nano Energy*, 2021, **85**, 105963.

8 L. Xu, W. Tao, H. Liu, J. Ning, M. Huang, B. Zhao, X. Lu and S. Tan, *J. Mater. Chem. A*, 2021, **9**, 11734–11740.

9 H. Feng, Y. Dai, L. Guo, D. Wang, H. Dong, Z. Liu, L. Zhang, Y. Zhu, C. Su, Y. Chen and W. Wu, *Nano Res.*, 2022, **15**, 3222–3229.

10 X. Liao, Q. He, G. Zhou, X. Xia, P. Zhu, Z. Xing, H. Zhu, Z. Yao, X. Lu and Y. Chen, *Chem. Mater.*, 2021, **33**, 430–440.

11 H. Wang, L. Yang, P. Lin, C. Chueh, X. Liu, S. Qu, S. Guang, J. Yu and W. Tang, *Small*, 2021, **17**, 2007746.

12 M. Guan, W. Tao, L. Xu, Y. Qin, J. Zhang, S. Tan, M. Huang and B. Zhao, *J. Mater. Chem. A*, 2022, **10**, 9746–9752.

13 Y. Yan, Y. Zhang, Y. Liu, Y. Shi, D. Qiu, D. Deng, J. Zhang, B. Wang, M. A. Adil, K. Amin, W. A. Memon, M. Wang, H. Zhou, X. Zhang and Z. Wei, *Adv. Energy Mater.*, 2022, **12**, 2200129.

14 C. An, Y. Qin, T. Zhang, Q. Lv, J. Qin, S. Zhang, C. He, H. Ade and J. Hou, *J. Mater. Chem. A*, 2021, **9**, 13653–13660.

15 B. Qiu, Z. Chen, S. Qin, J. Yao, W. Huang, L. Meng, H. Zhu, Y. (Michael) Yang, Z. Zhang and Y. Li, *Adv. Mater.*, 2020, **32**, 1908373.